

**ENGINEERED CEMENTITIOUS COMPOSITES (ECC) –
TAILORED COMPOSITES THROUGH MICROMECHANICAL
MODELING***

Victor C. Li

Advanced Civil Engineering Materials Research Laboratory,
Department of Civil and Environmental Engineering,
University of Michigan, Ann Arbor, MI 48109-2125, USA

Abstract: This article provides a brief overview of several classes of fiber reinforced cement based composites and suggests future directions in FRC development. Special focus is placed on micromechanics based design methodology of strain-hardening cement based composites. As example, a particular engineered cementitious composite newly developed at the ACE-MRL at the University of Michigan is described in detail with regard to its design, material composition, processing, and mechanical properties. Three potential applications which utilize the unique properties of such composites are cited in this paper, and future research needs are identified.

* To appear in Fiber Reinforced Concrete: Present and the Future, Eds: N. Banthia, A. Bentur, and A. Mufti, Canadian Society of Civil Engineers, 1997.

INTRODUCTION

The application of fiber reinforced concrete (FRC) can be grouped into two general classes: Thin sheet products and bulk structures. When FRCs are used in thin sheet products, such as cladding walls, roofing tiles, or pipes, they typically have the following characteristics (1): A high fiber volume fraction is used, often in the range of 3-10% with special processing methods (e.g. Hatschek, spray up, lay-up, extrusion and pultrusion processes) to accommodate the high fiber volume fraction. The fibers are often in continuous and aligned form (although one of the most successful form -- asbestos cement, has short random fibers in high volume), to take advantage of the simple geometric shape of the thin sheet product and to optimize the reinforcement efficiency of the fibers. As a result of this high efficiency and fiber volume fraction, this type of FRC often exhibits excellent mechanical performance in tension and bending, e.g. (2,3), to the extent that primary steel reinforcement is not needed. Alternatively, one can view the thin sheet product as one in which primary steel reinforcement is difficult to place, and therefore the FRC must be able to serve as primary load carrier. The excellent performance of this type of FRC is often reflected by its strain-hardening behavior beyond first cracking in tension. Despite this excellent performance, application of this type of FRC is limited by the simple geometric shape requirement. The pre-cast nature and special processing needs also restrict the extension of this class of FRC to applications in cast-in-place and bulk structures.

FRC applications in bulk structures can be subdivided into approximately three different classes, according to their fiber volume fraction and intended functions of the reinforcing fibers. Fibers in low fiber volume fraction (<1%) FRCs are often used for plastic shrinkage crack control. The fibers usually do not serve any structural functions. Moderate fiber volume fraction (between 1 and 2%) FRCs are versatile materials which can be found in both cast-in-place and pre-cast structural members. Because the fibers used are typically chopped and because of the low volume percentage, regular concrete mixing and casting processes can be employed. This type of materials are characterized by their improved modulus of rupture (MOR), fracture toughness, fatigue resistance, impact load resistance and other desirable mechanical properties (1,4). The fibers in such FRCs are often regarded as secondary reinforcement used in conjunction with main reinforcing steel. Attempts at partial replacement of shear steel reinforcement (e.g. 5–8) and reinforcement for crack width control (9,10) have been successful. Even so, the application of this type of FRC often find obstacles in cost/performance justifications. Recent progress at integrating structural performance with tensile characteristics of this type of FRC should place the cost/performance at an increasing advantage. For example, in an ongoing EU project, the tensile stress-crack width relationship of the FRC is taken into account in the design of a continuous FRC pavement overlay (11) for handling the expected thermal and mechanical tensile load. Similarly, in the design of tunnel linings (12), the tension-softening curve of the FRC is taken into account.

In recent years, techniques at placing large amount of fibers (between 5 and 20% by volume) into bulk structures such as beams, columns and connections have been successfully introduced. Some examples of high fiber volume fraction FRCs include SIFCON (5–20 % steel fibers, slurry infiltrated, (13,14)), SIMCON (6% steel fiber mat, slurry infiltrated (15); slurry infiltrated steel wool (16)) and CRC matrix (5–10% fine steel fibers (17)). These materials have excellent mechanical properties, including improvement in all strength properties, fracture toughness, and sometimes even appear to exhibit strain-hardening behavior as in some thin-sheet FRCs. Because of the significant improvement in mechanical properties, such high fiber volume FRCs often share primary importance with the main reinforcements in a given structural member. For example, they have been considered for providing structural ductility in over-reinforced R/C beams (18) and in brittle carbon FRP R/C structures (19). Despite their high performance, their wider application may be hindered by the special processing requirement due to their high fiber volume fractions and they are often restricted to precast members. These characteristics are common with those of thin-sheet products. The high cost and weight associated with the high fiber volume fraction are also important concerns. These materials are often restricted to steel fiber type. In addition, a number of researchers have pointed out the anisotropic properties (20) and existence of weak planes (21) in some of these materials due to fiber orientation effect associated with the material processing technique.

A major challenge to the research community is to develop a new type of FRC which has the favorable characteristics of the various classes of FRCs in use today and summarized above. These favorable characteristics should include:

1. Flexible processing – can be used in pre-cast or cast-in-place applications and no requirement of very special processing machinery.
2. Short fibers of moderate volume fraction – to maintain flexible processing, reduce cost and weight.
3. Isotropic properties – no weak planes under multiaxial loading conditions in bulk structures.
4. High performance – leading to significant improvements in strength, ductility, fracture toughness, and exhibit pseudo strain-hardening.

The fourth characteristics appear to be exclusive of the others, and current materials satisfy some but not all of these characteristics. Conventionally, research has focused on studying the property dependence of FRC on one or two parameters at a time, typically the fiber volume fraction, or fiber length. However, it is now well-known that composite properties depend on three groups of constituent properties – the fiber, matrix and interface properties (Table 1). The importance of this is the recognition that fiber volume fraction, for example, is only one of more than ten constituent parameters under our control for material engineering.

It is not enough to understand the individual influence of each parameter on composite properties, which can be (at least in principle) established empirically. Composite optimization requires that the combined influence of all relevant parameters on composite properties be known. Composite optimization can lead to

a composite with excellent performance with only moderate fiber volume fraction, thus meeting the favorable characteristics of an ideal FRC described above.

Table 1: Cement Based Fiber Composite Material Constituents and Their Properties

CONSTITUENTS	PROPERTIES
Fiber	Elastic modulus, tensile strength, length, diameter, volume fraction
Matrix	Fracture toughness, elastic modulus, initial flaw size
Interface	Bond properties, snubbing coefficient

To establish the combined influence of the constituent parameters on composite properties, it is necessary to develop a fundamental understanding of the micromechanisms which govern a given material property. (As a simple example, it is well known that the unstable propagation of a material defect in the form of a pre-existing crack governs the tensile strength of a brittle solid). Based on this understanding, it will be possible to identify the material microstructure and associated properties which control composite behavior. (The above example will lead to the defect size and intrinsic fracture toughness as micro-parameters governing the brittle material strength). Hence micromechanics serves to establish the link between material constituents and composite properties. The resulting information can be used to advantage for composite design. When fully developed, micromechanics can also be utilized as a tool for material property tailoring.

In this paper, we review some results of this micromechanics based approach (22–24) to engineering an FRC which shows pseudo strain-hardening, despite the relatively low fiber volume fraction (2% and less) and employing typical mixing and casting techniques. We have called this class of materials Engineered Cementitious Composites (ECC). In the following, we briefly review the conditions for pseudo strain-hardening, emphasizing the role played by each material constituent. Some mechanical properties of a specific ECC which should influence structural performance are summarized. Potential applications of this type of ECCs are indicated. Future research needs are then identified.

SYNOPSIS OF MICROMECHANICS BASED DESIGN METHODOLOGY

Micromechanical models constructed on the basis of fracture mechanics and deformation mechanisms provide an opportunity of tailoring microparameters so as to control the failure mode, the tensile strength, and ultimate tensile strain of the composite. Three types of tensile failure modes have been observed in cementitious materials (Fig. 1): brittle, quasi-brittle, and strain-hardening failure. Brittle failure can be observed in hardened cement paste material. It is characterized by a linear stress-strain curve (curve A) followed by a sudden drop in stress at first cracking with an ultimate tensile strain in the order of 0.01 %. Quasi-brittle failure can be observed in concrete and most fiber reinforced cements and concretes. It is characterized by a linear stress-strain curve (curve B) followed by a softening tail

after first cracking, due to the bridging action of aggregates, cement ligaments, and/or fibers. The ultimate tensile strain of quasi-brittle materials is of

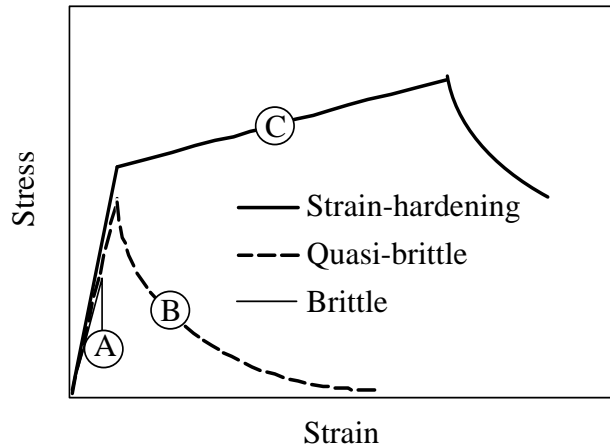


Fig. 1: Three Type of Failure Modes Observed in Cementitious Materials

the same order of magnitude as that for brittle materials. Strain-hardening materials are characterized by their ability to sustain increasing levels of loading after first cracking while undergoing large deformation (curve C). The ultimate strain value (at peak tensile load) of a strain-hardening material can be orders of magnitude higher than that of brittle or quasi-brittle material.

One of the most important conditions for the transition of quasi-brittle to strain-hardening failure mode is the presence of 'steady state' cracking (22–25). In fiber composites, the extension of a matrix crack is accompanied by fiber bridging across the crack flanks. As the matrix crack extends, the bridging zone increases in length. During crack opening, the bridging stress increases as fiber/matrix interfaces debond and the debonded segments of fibers stretch. When the bridging stress increases to the magnitude of the applied load, the crack flanks flatten to maintain the constant applied stress level (26). This load level is termed the steady state cracking stress. The crack has now gone into the steady state cracking mode, extending without the need of further increase in applied load. Thus during steady state cracking, the tensile load is independent of crack length. This is in contrast to the well known Griffith residual strength concept, which relates a decreasing tensile load to increasing crack size.

Based on a J-integral analysis of a steady state crack, Marshall and Cox (26) showed that

$$J_c = \sigma_{ss} \delta_{ss} - \int_0^{\delta_{ss}} \sigma(\delta) d\delta \quad (1)$$

where J_c refers to the crack tip toughness. In most fiber reinforced cementitious composites with less than 5% fiber volume fraction, J_c can be approximated as the cementitious matrix toughness. The steady state stress σ_{ss} and the flattened crack opening δ_{ss} are related via the bridging law $\sigma(\delta)$. The bridging law describes the relationship between the averaged stress carried by the fibers bridging across a matrix crack and the opening of this crack. For steady state cracking to occur at all, the steady state cracking stress must be less than the maximum bridging stress σ_o in the bridging law. That is,

$$\sigma_{ss} \leq \sigma_o \quad (2)$$

Eq. (1) and (2) together provide a general condition for transition from quasi-brittle to strain-hardening failure mode. Apart from steady state cracking condition, it is also necessary for the critical flaw size dependent first crack strength to be less than the maximum bridging stress (22). Otherwise, the bridging fibers will not be able to bear the tensile load shed by the matrix at first crack.

For Eq. (2) to be useful in fiber, matrix and interface tailoring, it will be necessary to determine the bridging law specific for a given composite system. In fiber reinforced cementitious composite in which the fibers are randomly oriented and in which pull-out (rather than fiber rupture) are expected, Li (27) shows that the bridging law can be derived as

$$\sigma(\delta) = \begin{cases} \sigma_o \left[2(\delta / \delta_o)^{1/2} - (\delta / \delta_o) \right] & \text{for } \delta \leq \delta_o \\ \sigma_o (1 - 2\delta / L_f)^2 & \text{for } \delta_o \leq \delta \leq L_f / 2 \\ 0 & \text{for } L_f / 2 \leq \delta \end{cases} \quad (3)$$

where $\delta_o = \tau L_f^2 / (E_f d_f (1 + \eta))$ is the crack opening corresponding to the maximum bridging stress

$$\sigma_o = \frac{1}{2} g \tau V_f \frac{L_f}{d_f} \quad (4)$$

Corresponding equations for cases where fibers can rupture and for cases where fibers are of variable length can be found in (28, 29). In Eqs. (3) and (4), V_f , L_f , d_f and E_f are the fiber volume fraction, length, diameter and Young's Modulus, respectively. τ is the fiber/matrix frictional bond strength, and the snubbing factor

$$g = \frac{2}{(4 + f^2)} (1 + e^{f\pi/2}) \quad (5)$$

where f is a snubbing coefficient which must be determined experimentally for a given fiber/matrix system. The snubbing coefficient raises the bridging stress of fibers bridging at an angle inclined to the matrix crack plane, appropriate for flexible fibers exiting the matrix analogous to a rope passing over a friction pulley. Finally, $\eta = (V_f E_f)/(V_m E_m)$, where V_m and E_m are the matrix volume fraction and Young's Modulus, respectively.

The condition for steady state cracking expressed in Eq. (2) can now be interpreted as a critical fiber volume fraction above which the composite will show pseudo strain-hardening. Using (1) and (3) in (2), this critical fiber volume fraction can be defined in terms of the fiber, matrix and interface parameters (24):

$$V_f^{crit} \equiv \frac{12J_c}{g\tau(L_f/d_f)\delta_o} \quad (6)$$

Equation (6) is important for composite design. It provides guidelines for tailoring the microparameters such that V_f^{crit} is minimized. Strain-hardening composites can then be designed with the minimum fiber content. This idea is further explained below:

1. Tailoring of Matrix Toughness: Smaller amount of fiber is needed to make the transition from the quasi-brittle failure mode to the strain-hardening failure mode if the matrix toughness J_c is small. This has implications on matrix design since the toughness can be controlled by the water/cement (w/c) ratio, the volume, size and type of aggregates and microfillers such as silica fume (30). However, it must be noted that too low a matrix toughness will lead to a low first crack strength, undesirable for normal service loads.

2. Tailoring of Interfacial Bond: Improving the frictional bond property τ , but without causing fiber breakage, will lead to mode transition at lower fiber volume fraction. The ductility of the composite is associated with the inelastic strain generated as a result of multiple cracking (22). This inelastic strain results from the multiple crack density, and from the opening of each crack. The multiple crack density is expected to increase with the bond strength τ , which controls the rate of stress transfer from the bridging fiber into the matrix material. Fiber/matrix interface bond properties can be altered by fiber surface modification, fiber deformation, and transition zone modification.

3. Tailoring of Fiber Length: Eq. (6) suggests that the fiber length L_f plays a crucial role since V_f^{crit} scales inversely with the third power (approximately, becomes exact only for low V_f case due to the η -term in δ_o) of L_f . (Note that δ_o scales with the square of L_f). While long fibers are preferred, difficulty in processing because of poor workability puts a limit on the choice of fiber length. Further, long fiber length can lead to fiber rupture and poor post-peak behavior. On

the other hand, it may not be necessary to use this post-peak behavior if the material strain-hardens which already provides structural ductility.

Once the failure mode transition is assured, the ultimate strength σ_{cu} of the strain-hardening composite can be identified with the maximum bridging stress σ_o given in Eq. (4). That is,

$$\sigma_{cu} = \sigma_o \quad (7)$$

Hence the ultimate composite strength can also be controlled by tailoring the fiber volume fraction, the interface frictional bond strength, and the fiber aspect ratio L_f/d_f , according to (4) and (7). The ultimate strength is not affected by the matrix properties.

To facilitate composite constituent selection, design charts (30) such as that shown in Fig. 2 can be used in lieu of Eq. (6).

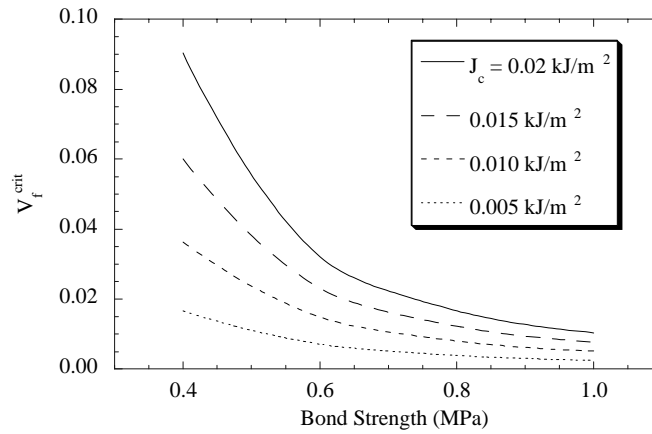


Fig. 2: Matrix Toughness & Interfacial Property Effect on Critical V_f . ($E_f = 120$ GPa, $L_f = 12.7$ mm, $d_f = 0.038$ mm, $g = 2.0$, $E_m = 25$ GPa)

MATERIAL

ECCs can be formed with a variety of fibers, including polymeric (23), steel (31) and carbon (29). The matrices used are mostly cement and mortar. So far, most research has been conducted with a high modulus polyethylene fiber (Trade name Spectra 900) in a cement matrix, and this material forms the basis of discussions in this paper. The properties reviewed below involves Spectra ECCs the composition of which has varied somewhat from test to test, carried out over the last six years at the University of Michigan. Typical material composition and mix proportions are given in Table 2. For the exact mix design, the reader is referred back to the original publications. Fiber properties are given in Table 3. Most mechanical properties described below are for a composite with 2% of fibers by

volume. For comparison purposes, corresponding properties of a typical FRC containing 1% of (ZL 30/50 hooked end) steel fibers are also shown.

Table 2: Material Mix Proportions

MAT'LS	CEMENT	SILICA FUME	SUPER-PLASTICISER	W/C	AGGREGATES FA/CA
ECC	1.0	0.10 – 0.20	0.01– 0.03	0.30 – 0.32	–
FRC	1.0	–	–	0.45	1.73/1.73

Table 3: Polyethylene Fiber Dimensions and Mechanical Properties

FIBER DIAMETER (μm)	FIBER LENGTH (mm)	ELASTIC MODULUS (GPa)	FIBER STRENGTH (MPa)	FIBER DENSITY (g/cm^3)
38	12.7	120	2700	0.98

The interfacial bond property τ has been measured (32) both by single fiber pull-out test as well as by back calculation based on ultimate strength measurement (using Eq. (4)). The range of $\tau = 0.5$ to 0.7 appears typical for the type of matrices used. It is known to depend on age, matrix composition, and even fiber volume fraction. This low bond property can be increased by a factor of two or more by means of plasma treatment (32). The snubbing factor g has not been measured for this material system, although polypropylene and nylon fibers in cementitious systems show snubbing factors of 1.8 and 2.3, respectively (33). For the present purpose, a value of $g = 2$ has been assumed.

The fracture toughness K_m measured using LEFM techniques (34) yields a value of $0.33 \text{ MPa}\sqrt{\text{m}}$. The elastic modulus E_m has been estimated (30) using Hirsch's formula to be about 23 GPa, based on its age and w/c ratio.

Using Eq. (6) and the above parametric values, the critical fiber volume fraction is estimated between 0.5 % and 1%. It should be understood that this is a rough estimate, since the exact in-situ values of matrix and interface parameters has not be measured directly. At any rate, the critical fiber volume fraction is well below 2%. Hence a composite with 2% fiber should satisfy the condition of pseudo strain-hardening, and exhibit high strain capacity after first cracking.

The polyethylene fibers are supplied by the manufacturer in bundle-like form. Prior to mixing, the fibers were dispersed using air pressure for approximately one minute. Then the amount of fibers needed for the mix was weighted. After measuring the weight of all mix constituents, the cement was poured into a three speed (Hobart) mixer with a planetary rotating blade. Silica fume was slowly added to the cement when the mixer has been started. Then water and superplasticizer were mixed together and slowly added. When all water and superplasticizer were added and the cement paste mix became uniform, the

dispersed fibers were slowly added by hand to the mix. The total mixing time was between 15 to 30 minutes depending on the batch size and the amount of fibers used (fiber volume fraction). After the mix was ready, the specimens were cast under high frequency vibration (150 Hz) in already greased Plexiglas molds. Subsequently, they were covered with a polyethylene sheet and allowed to harden at room temperature for one day prior to demolding. The specimens were placed in a water curing tank for 4 weeks following the demolding process, and then removed from water and prepared for testing. For most specimens, a thin white coating of lime was applied on the specimens prior to testing to better monitor the development of cracks. The age at testing of the specimens was 30 to 60 days.

MECHANICAL PROPERTIES OF ECC

Uniaxial tensile test, compression test, flexural test and fracture test have been carried out for ECCs at the ACE-MRL. In each case, the test conditions, specimen and loading configuration, pertinent stress-deformation curves, and failure pattern on the specimens are summarized here. A compendium of mechanical properties obtained so far for the ECC described above is given in Table 4. For comparison purpose, similar data for FRC tested under the same conditions are also included in this table.

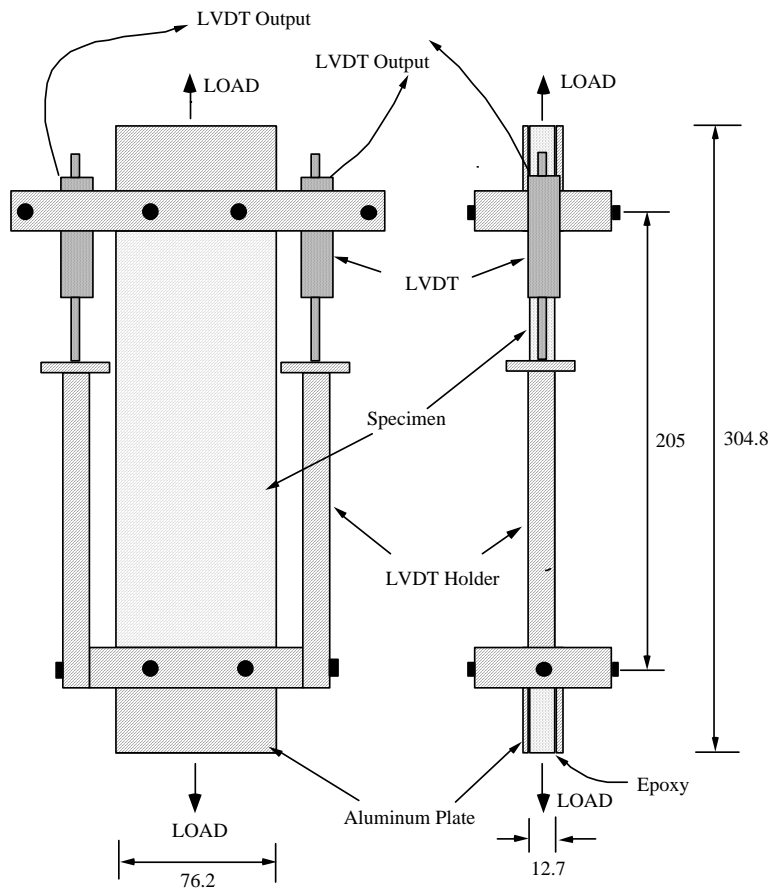
Table 4: Properties of ECC and FRC

	Tensile				Compressive		Stiff-ness	Flex-ural	Fract-ure
	σ_{fc} (MPa)	ϵ_{fc} %	σ_{cu} (MPa)	ϵ_{cu} %	f'_c (MPa)	ϵ'_c %	E (GPa)	MOR (MPa)	J (kJ/m ²)
ECC	2.5	0.021	4.6	5.6	68.5	0.67	22	25	27
FRC	4.3	0.035	4.3	0.035	55	0.48	32.5	10.9	4.9

Uniaxial Tensile Behavior

The uniaxial tensile specimens were tested under displacement control (loading rate ~ 0.005 mm/s) in a 133.5 kN capacity MTS 810 material testing system with hydraulic wedge grips. Aluminum plates were glued onto the ends of the tension specimens to facilitate gripping. Two linear variable differential transducers (LVDT's) with gage length of 207 mm were used to measure tensile deformation on the specimen surface (see Fig. 3). More details of the uniaxial tension test set up can be found in (31).

Figure 4 shows the stress-strain curves recorded on uniaxial tension specimens. The ECC shows clear pseudo-strain hardening behavior with average strain at peak stress ϵ_{cu} approximately equal to 5.6 % (about 560 time the strain capacity of the unreinforced matrix). The first crack strength σ_{fc} and strain ϵ_{fc} are



All dimensions are in mm

Fig. 3: Tensile Coupon with LVDT Holder Mounted Before Test

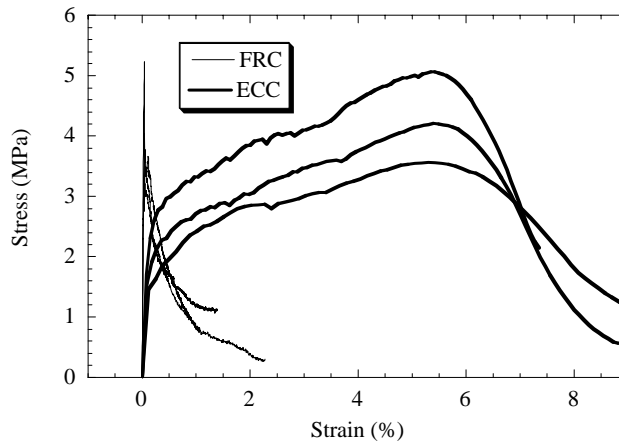


Fig. 4: Uniaxial Tensile Stress-Strain Response of ECC with FRC

2.5 MPa and 0.021 %, respectively. The ultimate tensile strength σ_{cu} is 4.6 MPa. For this composite, real-time observation showed that multiple cracking occurred with many sub-parallel cracks across the specimen during strain-hardening. Beyond peak stress, localized crack extension occurred accompanied by fiber bridging. For comparison, the stress-strain curves for a 1% steel FRC are also shown in this figure. This material reveals the typical quasi-brittle behavior of most FRCs. The softening branch is not a true strain, but reflects the increasing opening of a single crack (divided by the gage length of the LVDT).

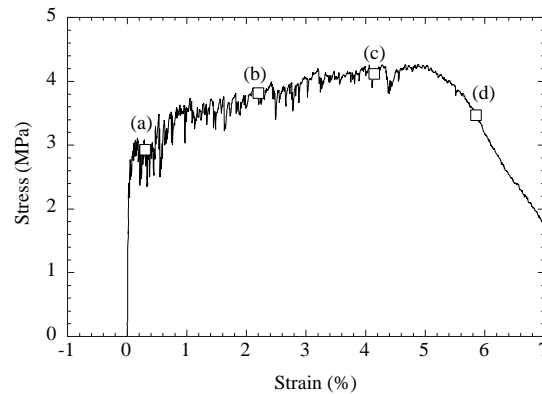


Fig. 5: Uniaxial Tensile Stress-Deformation Record for ECC

Figure 6 shows an example of a damage record at four different stages of loading (see Fig. 5). As indicated in this figure, although the specimen is already cracked at stage (a) beyond the first crack strength, the material continues to sustain the applied load. At stage (b), at about half the maximum strain capacity, more cracks have developed in the specimen, but the material is still capable of resisting higher levels of loading. As further deformation is imposed on the specimen, additional cracking takes place, with saturation approached near peak load (stage (c)). At stage (d), a single macrocrack has already localized in the specimen and the material has started to soften. The actual macrocrack was not recorded, but it has occurred in a location close to the one shown at the top of Fig. 6(d).

Compressive Strength

Compression cylinders (7.62mm x 15.24mm) were tested in an Instron Model 8000 test system with a 2500 kN capacity loading frame (30). Each cylinder was tested under displacement control at a loading rate of 0.0254 mm/s.

Compressive stress-strain curves for the ECC and FRC are shown in Fig. 7. The compressive strength of this ECC, about 68.5 MPa, is not significantly higher than that of the FRC (55 MPa). The compressive strain capacity has been observed to increase by approximately 50%-100% over normal concrete and FRCs. Post-peak ductility of ECCs are expected to be similar to that of normal FRCs.

The modulus of ECC, as in ordinary concrete, depends on the amount of aggregates used. However, the presence of aggregates also changes other properties

of the matrix in the ECC composite. Careful control of aggregate content and size is of paramount importance in the design of ECCs. The modulus of this ECC has been measured by strain gages as 20.3 MPa. Higher modulus, but without sacrificing tensile strain-hardening has been achieved (30).

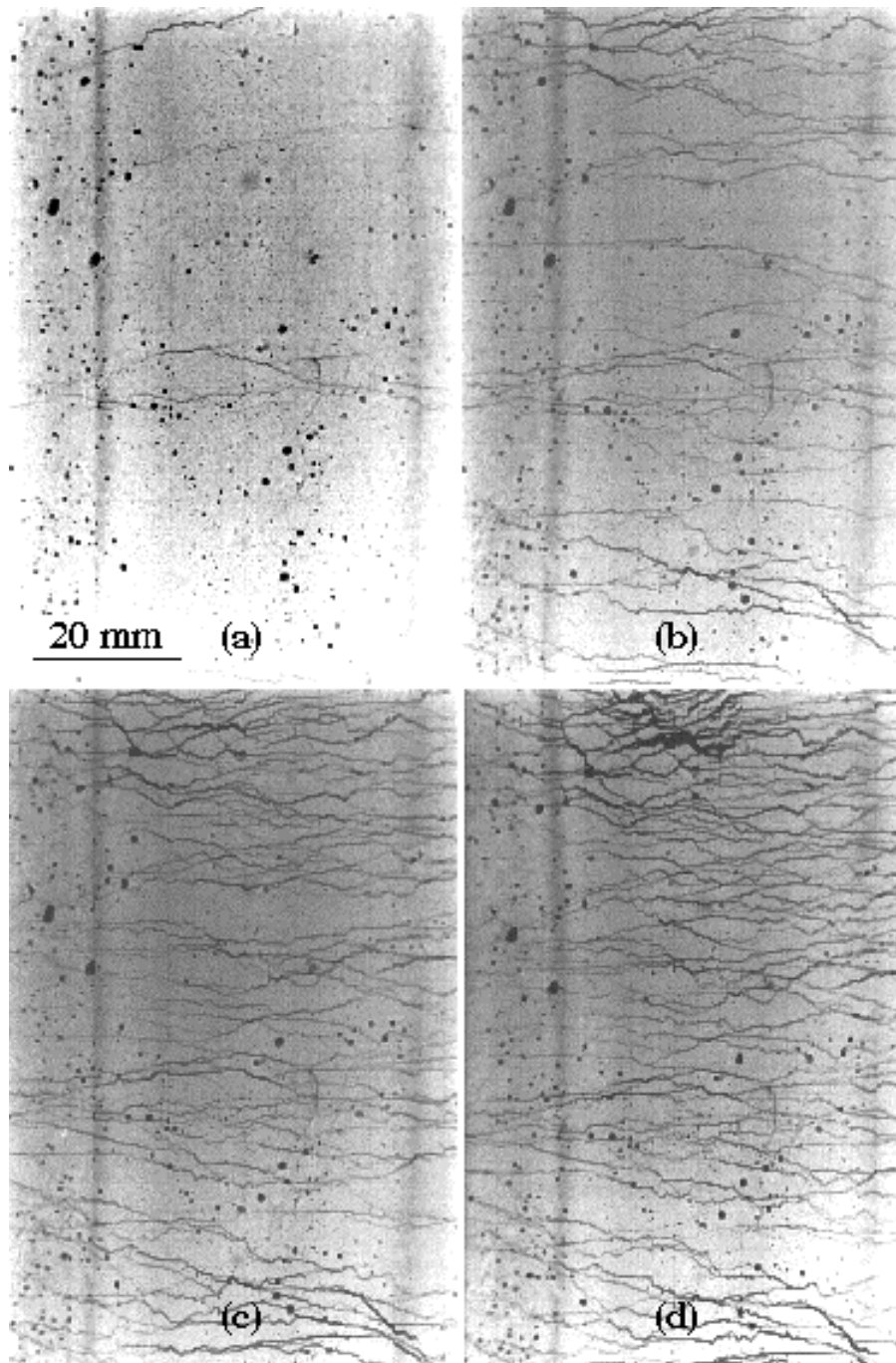


Fig. 6: Damage Evolution on Uniaxial Tensile Specimens at

(a) $\epsilon = 0.3\%$, (b) $\epsilon = 2.2\%$, (c) $\epsilon = 4.2\%$, (d) " ϵ " = 5.9%

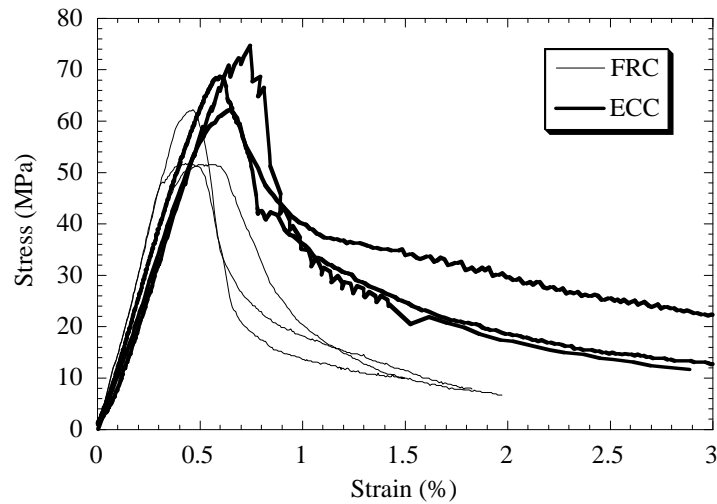


Fig. 7: Compression Stress-Strain Curves of ECC and FRC

Modulus of Rupture

The geometry and loading configuration of the flexural beam specimens are shown in Fig. 8. This experimental set-up is recommended in ASTM C78-75, standard test method of flexural strength of concrete (using simple beam with third-point loading). The flexural tests were conducted in the same MTS testing system as the uniaxial tensile tests. The specimens were loaded to complete failure with a constant cross head speed (0.01 mm/s). The load, head displacement of the machine, and deflection of the beams at the middle point were recorded in each test. More details of the test set-up can be found in (35).

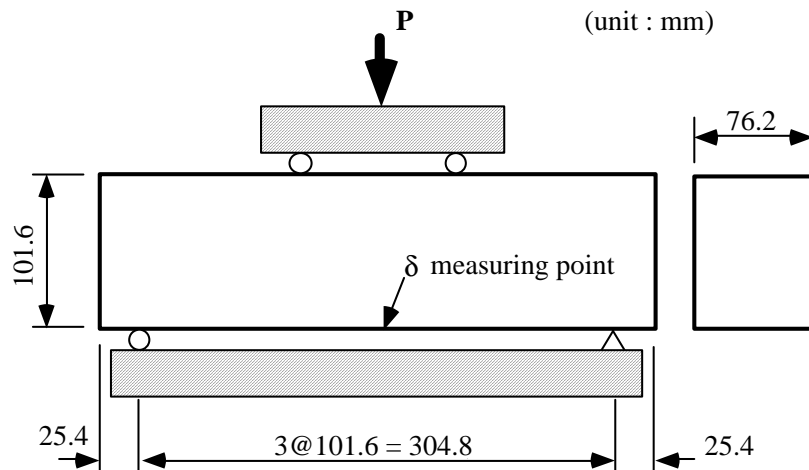


Fig. 8: Geometry of Bending Specimens

The flexural stress-deflection curves of the ECC are shown in Fig. 9. For comparison, the stress-deflection curves for a 1% steel FRC are also shown. For the steel FRC, the flexural stress increases rapidly to the peak value and then starts to decay. The average beam deflection at peak stress is about 0.6 mm. For the ECC, however, the flexural stress increases at a slower rate. This increase is accompanied by the development of multiple fine cracks. The average beam deflection at peak stress is about 7.4 mm. The flexural strength (MOR) for the ECC is determined to be 12.5 MPa, compared to 10.9 MPa for the steel FRC. Although toughness index has not been measured for the ECC, it is expected to be much higher than the FRC based on the area under their flexural stress-deflection curves.

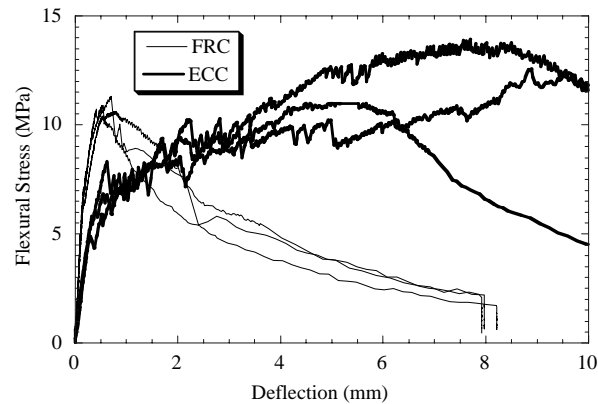


Fig. 9: Flexural Stress-Deflection Curves of ECC and FRC

The crack pattern of the ECC is distinctly different from plain concrete or normal FRC. The first crack started inside the mid-span at the tensile face, and multiple cracks developed from the first cracking point and spread to the outside of the mid-span. The multiple cracks in the outside of the mid-span were inclined cracks similar to shear cracks in steel reinforced concrete (R/C) beams. As the MOR is approached, one of the cracks inside the mid-span started to open up after a large damage zone had been developed. The through-thickness damage zone can reach an areal dimension of 200 cm². Fig. 10 shows a typical cracking pattern that develops in the beam middle span around the peak load.

For ideally brittle material, the MOR to tensile strength ratio is unity. For quasi-brittle material such as concrete or FRC, this ratio lies between 1 and 3. The upper limit describes the case of a elastic-perfectly plastic material. For the case of ECC, this ratio can be expected to be higher than 3 due to the strain-hardening nature after first crack. This expectation is confirmed by the test results (35, 36) which show that the ratio is equal to 5.0 for the ECC, compared to 2.5 for the FRC.

Fracture Energy

Fracture toughness tests of ECCs (34, 37) were conducted in the same MTS testing system as the uniaxial tensile tests. Double cantilever beam (DCB) specimens of size shown in Fig. 11 was used to determine the fracture energy of the composite. A clevis and pin arrangement (similar to that recommended by ASTM

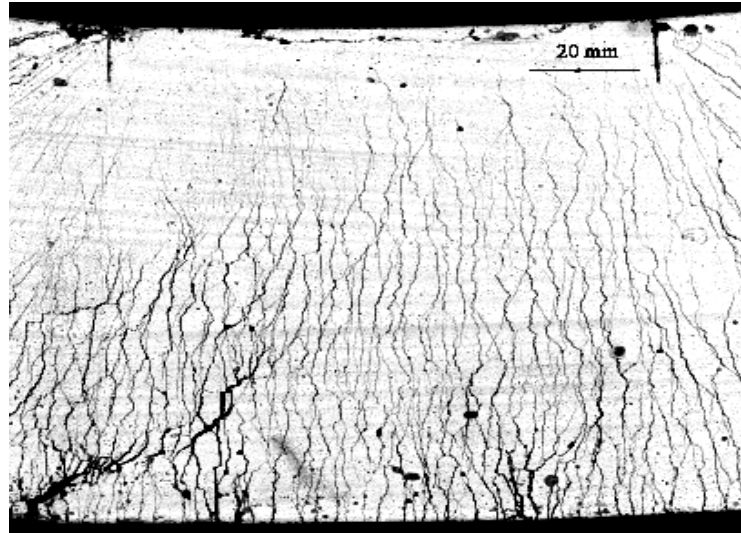


Fig. 10: Cracking Pattern in ECC Beam Mid-Span Around Peak Load

E399-78) was employed at both the top and bottom of the DCB specimens to allow rotation as the specimens were loaded. The specimens were loaded to complete failure with a constant cross head speed; the testing time was typically 40 minutes for all tests. The load-line displacement δ_L was measured using two LVDTs. The total fracture energy was determined by means of the J-based technique described by Li et al (38) and using a set of DCB specimens with different notch lengths. Concurrently with the tests, damage evolution on the specimen surface was recorded using a camera. The size of the specimen has been chosen to ensure steady state crack growth.

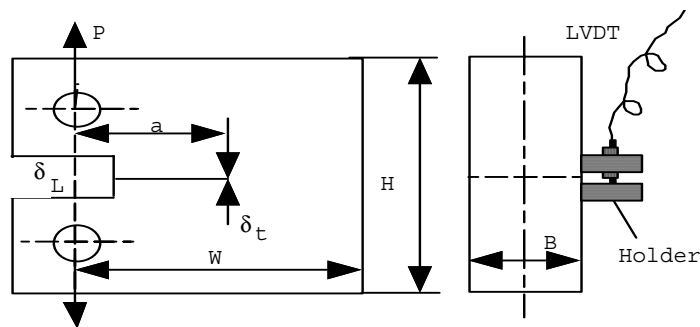


Fig. 11: Geometry of Fracture Specimens
 Large (W = 490 mm; H = 585 mm; B = 35 mm)
 Small (W = 127 mm; H = 153 mm; B = 35 mm)

Figure 12 shows an example of load-displacement curves recorded for the DCB fracture specimens. For the ECC material, it is seen that despite the presence of the deep notch the material produces significant damage tolerance subsequent to the bend-over point. Fig. 13 presents the damage evolution recorded for various load-line deformation values indicated in Fig. 12. It is particularly noted that an extensive microcrack damage zone spreads around the notch tip before the localized crack starts to grow. Significant energy absorption is therefore expected from the off-crack-plane volumetric inelastic deformation process. For the FRC material, small non-linearity was observed prior to reaching the peak load. Then, the DCB specimen failed in a quasi-brittle manner by opening of a single macrocrack bridged by steel fibers. Note that the specimen size used for the FRC is smaller than that used for the ECC. The larger specimen size used for the ECC material was necessary to achieve steady-state off-crack-plane cracking in the specimens (34).

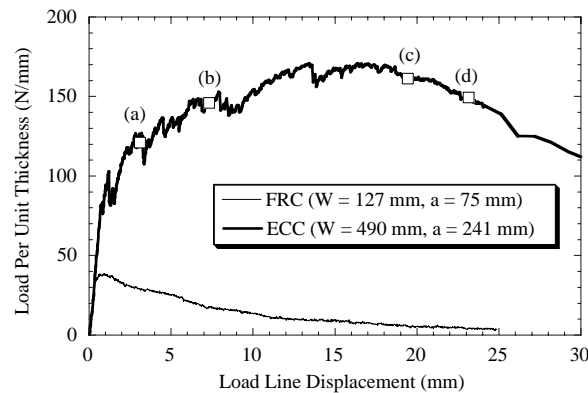


Fig. 12: DCB Load-Displacement Record for ECC and FRC

The total fracture energy measured for this ECC was 27 kJ/m^2 , with approximately over half of this energy consumed in the inelastic damage process occupying an area of 1150 cm^2 around the crack tip, and the rest coming from the pull-out of fibers on the crack wake. It is noted that in normal FRC, only the pull-out mechanism of fracture energy absorption is available. Li et al (36) pointed out that this difference in energy absorption mechanism is responsible for the much sharper rise in R-curve of ECCs compared to normal FRCs. The fracture energy of the FRC in this study has been measured to be 4.9 kJ/m^2 .

POTENTIAL APPLICATIONS

ECCs are relatively new materials. Although further refinement and optimization are expected, preliminary considerations suggest that the material can

be used to advantage in a number of applications. From Table 4, it is clear that the strength properties of this ECC are comparable to those of high strength concrete, while the deformation, crack width control, and energy absorption capacities are significantly improved because of the strain-hardening phenomenon. Applications in which such properties play an important role in improved performance can take advantage of ECCs. In the following we describe an example of each of these classes of applications. The application of ECC as patch repair material is currently under investigation at the University of Michigan.

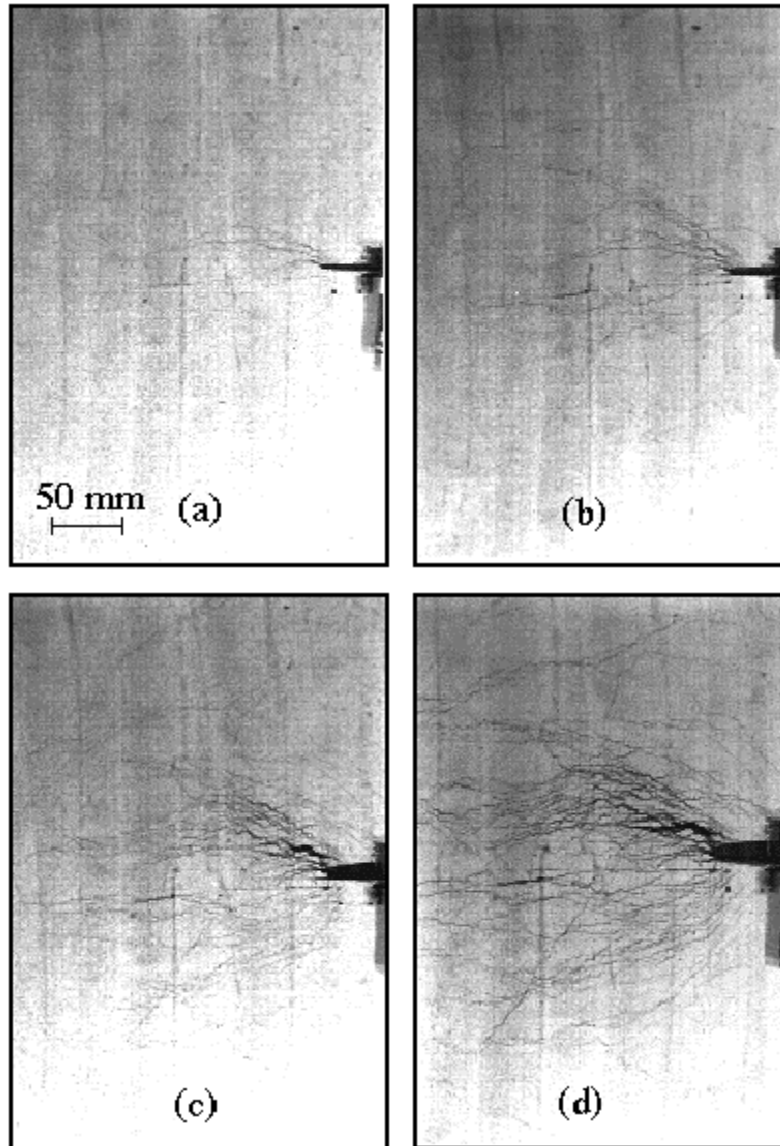


Fig. 13: DCB Damage Evolution as a Function of Deformation
(a) $\delta_L = 3.10$ mm (b) $\delta_L = 7.32$ mm (c) $\delta_L = 19.45$ mm (d) $\delta_L = 23.16$ mm

Concrete Elements Subjected to Shear

Shear failure is generally brittle in concrete structures. Examples of concrete structural failure related to shear loading includes bridge deck punching failure (39) corbel failure (40), anchor bolt pull-out (41) and segmental bridge shear key failure (42). Since shear failure often involves diagonal tensile cracks, it is expected that ECC structural members should reflect improve ductility under shear.

The Ohno shear beam configuration (43) was chosen to establish the shear performance of ECCs (44). Performance contrast with plain concrete, conventionally reinforced concrete, and ordinary fiber reinforced concrete was established. The geometry and loading arrangements are indicated in Fig. 14. The flexural steel has been designed to prevent flexural failure in the shear panel and ensure a shear mode of failure. The flexural reinforcement layout is shown schematically. Since a state of pure shear stress exists at the centroid of the specimen, the Ohno shear specimen gives an estimate of shear strength that is closer to the actual shear strength of the material as compared to the conventional two point loading shear beam test.

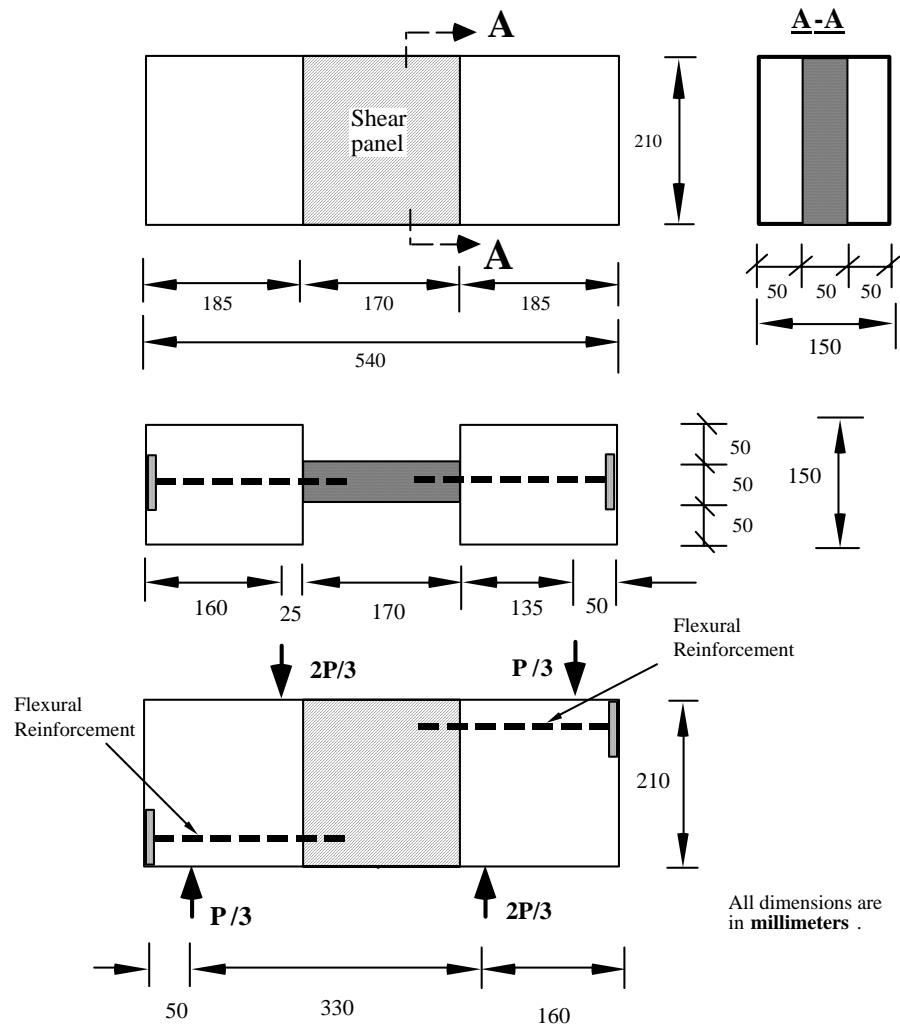


Fig. 14: Ohno Shear Beam Geometry and Loading Configuration

The Ohno shear beams were tested in an Instron Model 8000 test system with a 500 kN capacity loading frame. Tests were run under displacement control at a loading rate of 0.381 mm/min. Total test time was approximately 10 minutes. The loads were applied through rollers resting on 25.4 mm wide thin aluminum spreader plates glued to the specimen. The beams were placed on roller supports.

The shear load versus deflection curve is shown in Fig. 15. Beam deflection was measured by a LVDT located under the interior load point. After first crack strength, the ram load continued to increase. The pseudo strain-hardening behavior of ECC revealed itself in the form of multiple diagonal cracks (Fig. 16) with small crack widths of less than 0.1 mm even up to ultimate load. In contrast, the FRC beam failed shortly after first crack load with a single crack opening as the crack width increased at continuously softening load. It is clear from Fig. 15 that the ductility of the ECC beam is extensive both pre-peak and post-peak. Indeed Li et al

(44) showed that the ductility of this ECC beam is even better than a similar beam with conventional shear reinforcement in the form of a welded steel wire fabric. In the FRC and especially in the conventionally shear reinforced beam, extensive spalling of concrete was observed after first cracking. This does not occur in the ECC beam, in spite of the large ductility shown in Fig. 15.

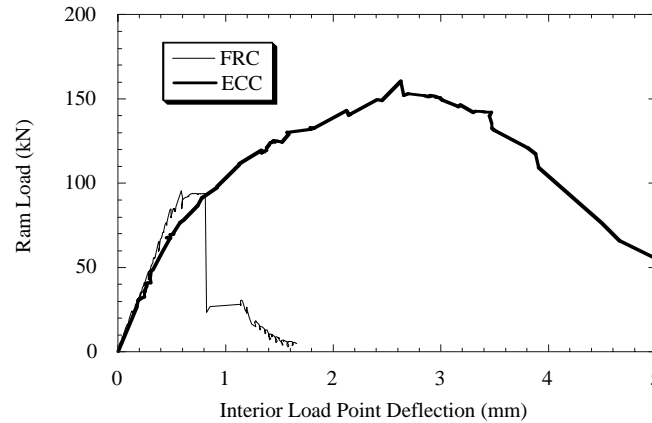


Fig. 15: Ram Load versus Deflection Curves of ECC and FRC Ohno Shear Beams

The average shear strength in the Ohno shear beams was estimated as the shear force at the beam center line (which is one-third of the ram load) divided by the cross-sectional area resisting the shear force. The ECC system failed at a stress of 5.09 MPa, compared to 3.03 MPa for the FRC. The unique ductility gain in the ECC beam is reflected by the average shear strain of 2.6% at ultimate load compared to 0.6% for the FRC.

The ductile shear response in ECC suggests that ECCs can be utilized in structures where intense shear loading can be expected, such as experienced by some concrete bridge decks (45), in concrete elements connected by steel anchors, and where conventional shear reinforcement is desired but prevented from adoption due to reinforcement congestion or otherwise.

Crack Width Control in R/C Beam

Maalej and Li (46) proposed a new design for reinforced concrete flexural members for the purpose of improving their durability. The design makes use of the unique strain-hardening property of ECCs to limit the crack width. The composite is used as a replacement for the concrete material that surrounds the main reinforcement in a regular reinforced concrete member. With this design it was shown that crack widths under service load conditions can be limited to values that could never be achieved using conventional steel reinforcement and commonly used concrete. Under these conditions, it was concluded that it would be possible to prevent the migration of aggressive substances into the concrete or the reinforcement. Furthermore, accelerated corrosion due to longitudinal crack or

spalling will be reduced if not eliminated, and spalling and delamination problems common to many of today's reinforced concrete structures will be prevented.

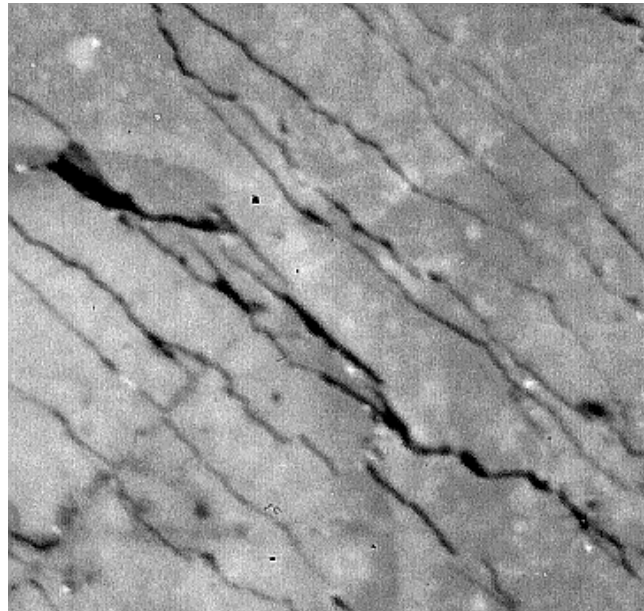


Fig. 16: Crack Pattern of Shear Panel, After Peak Load Reached

In the proposed design of the R/C member, a layer of ECC is substituted for the concrete that surrounds the main flexural reinforcement (Fig. 17). This ECC layered beam has the same cover thickness as for a control specimen, which has a regular concrete cover. Two performance requirements are imposed on the ECC material to serve its intended purpose: (1) the ultimate tensile strain capacity of the ECC material should be greater than the maximum strain that can be developed in the outermost fiber at the tensile face of the R/C beam, and (2) the crack width at the ultimate strain capacity of the ECC material (hereafter referred to as ultimate crack width) should be less than the maximum crack width allowed in a particular environment. The first condition ensures that no strain localization will take place in the ECC layer, and the second condition ensures that the crack opening in the ECC is maintained below the allowable value. Assuming that at ultimate load, the strain in the extreme compression fiber of the concrete is equal to 0.003, and that plane sections remain plane, the strain in the extreme tension fiber of the ECC is found to be equal to 0.013. Therefore, the ECC that should be selected should have an ultimate strain capacity at least equal to 0.013. In addition, suppose that the member is to be exposed in an environment of seawater and seawater spray under wetting and drying. In this case, according to ACI Committee 224, the crack width should be limited to 0.15 mm. Therefore, the ultimate crack width of ECC should be less than 0.15 mm. The 2% Spectra ECC discussed above was found to satisfy

the prescribed performance requirements and was selected as the material for the ECC layer (note that the average ultimate crack width for this material is 0.14 mm).

The beams were tested in an Instron Model 8000 test system with a 500 kN capacity loading frame. The tests were run under displacement control, and the total test time was approximately 15 minutes (loading rate approximately .025 mm/sec). Ram load and head displacement information were recorded. Four LVDTs were used to measure the beam deflection and curvature during loading.

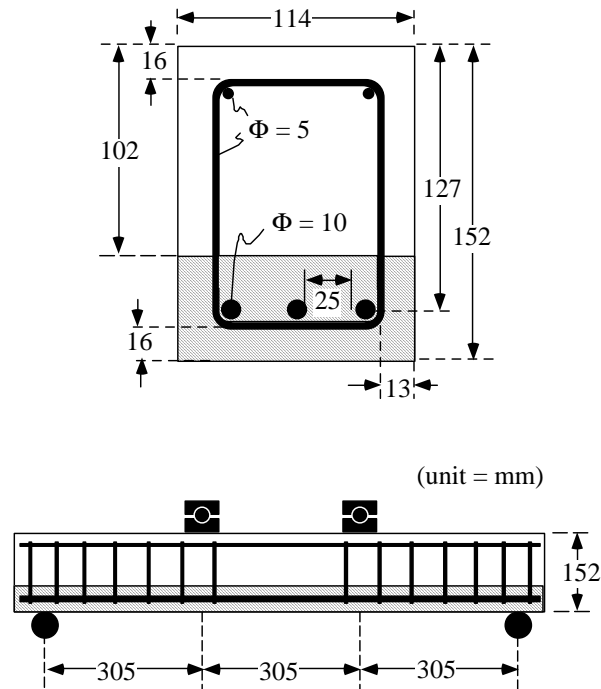


Fig. 17: Geometry of the R/C beam with ECC layer and reinforcement details

Figure 18 shows the test results, in the form of moment curvature and crack width curvature diagrams, for both beams. As shown in this figure, there is no significant difference between the moment curvature response of the two beams. The beam with the ECC layer shows a 10 % higher load and curvature at failure. The crack width-curvature response of the two beams is, however, significantly different. Fig. 18 shows that the crack width in the control specimen increases almost linearly as function of curvature. Before yielding of the reinforcement (moment ≈ 10.7 kN-m) the width of the crack at the bottom of the beam is maintained below 0.20 mm. After yielding, the load starts to increase at a much slower rate while the crack width continues to increase at the same rate. At peak load the width of the crack is approximately equal to 1.52 mm. For the ECC layered beam, the crack width maintains a small value at all times. The crack width first starts to increase almost linearly as function of curvature, and then actually decelerates at higher curvatures. Before yielding of the reinforcement (moment \approx

10.7 kN-m) the crack width is maintained below 0.05 mm. At ultimate load the crack width reaches 0.19 mm. Also the strain measured in the ECC material at the bottom of the beam was 0.026 which is smaller than the ultimate strain capacity of the material (0.055).

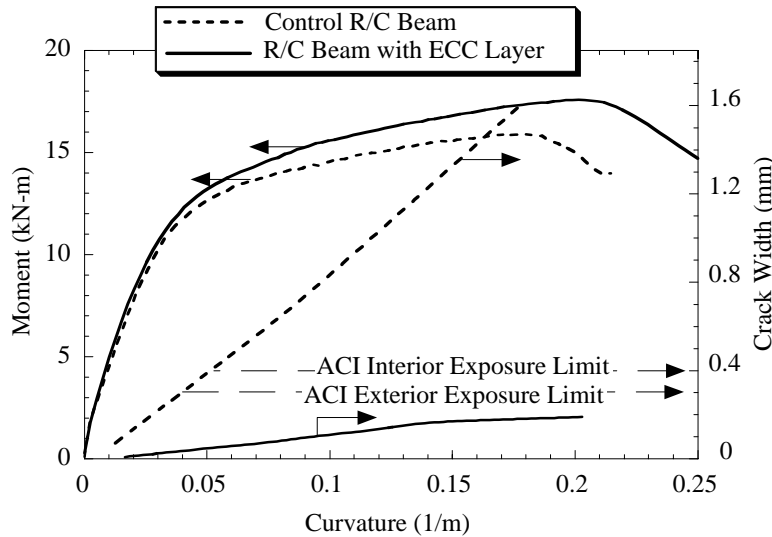


Fig. 18: Moment and Crack Width-Curvature Diagrams

Fig. 19 shows two series of pictures illustrating the increase of crack width as function of load for both the control R/C beam (series a) and the R/C beam with the ECC layer (series b). The load level is indicated on the bottom of each picture. These series of pictures indicate a significant difference in the cracking behavior of the two beams. They illustrate that for a given load level, the crack width in the ECC layered R/C beam is always smaller than that in the control specimen, and that the rate of crack width increase as function of load is much higher for the latter.

The overall crack patterns of the beams are shown in Fig. 20. For the control R/C beam, the commonly observed crack pattern (Fig. 20a) with tensile cracks emanating from the concrete cover was observed. For the ECC layered beam, the cracks in the concrete material diffused into many fine cracks when they met the ECC layer (Fig. 20b). This phenomenon appears similar to the crack pattern observed in Double Cantilever Beam (DCB) fracture specimens (Fig. 13). When a large crack develops in concrete it is accompanied by a strain concentration at the location where this crack meets the ECC material. Because of the stress transfer capability of the reinforcing fibers in the ECC material, stress redistribution occurs so that localized fracture is delayed. In fact, localized fracture may never develop in the ECC layer if the maximum strain in the layer is kept below the material ultimate strain capacity. Consequently, an expanded zone of matrix cracking must develop in the ECC layer prior to localized fracture.

Tsukamoto (47) determined that fluid flow rate scales with the third power of crack width in concrete. Based on the above results, one could conclude that the flow of aggressive substance into the ECC layered R/C member could be significantly reduced, thus slowing down corrosion rate. Note that this reduction in crack width is achieved without reducing the concrete cover thickness, considered to be important in structural durability (48).

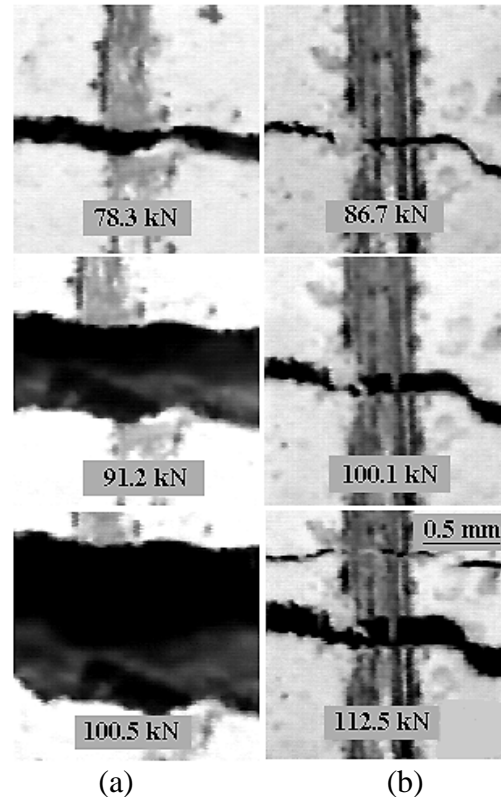


Fig. 19: Variation of Crack Width as Function of Load: (a) Control R/C Beam; (b) R/C Beam with ECC Layer

The corrosion of a reinforcing bar is accompanied by the production of iron oxides and hydroxides which occupy a volume larger than the original metal. As a result, a large pressure is exerted on the surrounding concrete which results in local radial cracks. These cracks can propagate along the bar, producing longitudinal cracks (49), spalling of the concrete, and potential loss of strength in the R/C member. In addition, a large crack may form parallel to the concrete surface at a plane of bars, resulting in the delamination of the surface, a serious problem in bridge decks. When the concrete that surrounds the reinforcement is replaced with ECC material, the longitudinal cracks are likely to be arrested before reaching the exposed surface, or otherwise be limited in width. In this case the control of the width of longitudinal cracks can be very effective in reducing the corrosion of the reinforcement. Moreover, by the use of an ECC, the spalling and delamination of

concrete will be eliminated. This is due to the high fracture resistance of the ECC material associated with a rapid rising R-curve. These potential benefits of ECC in structural applications remains to be laboratory and field tested.

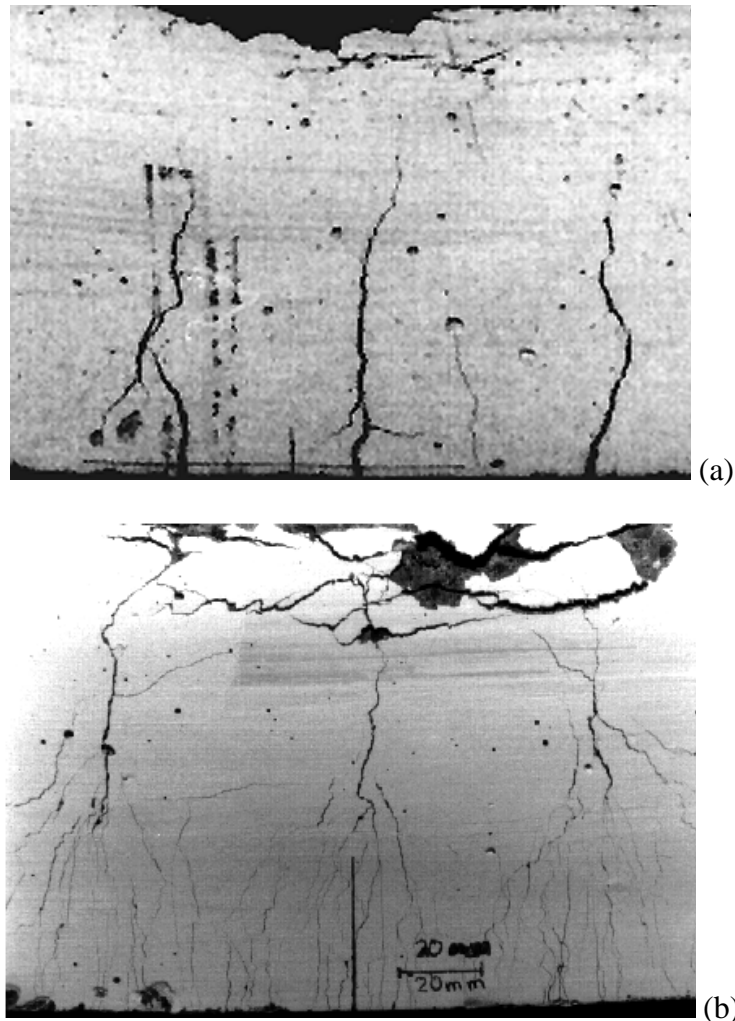


Fig. 20: Crack Pattern (a) Control R/C Beam; (b) R/C Beam with ECC Layer

Energy Absorption In Plastic Hinge Of Beam-Column Connection

In earthquake resistant design, the structural system performance requirements can be specified in terms of minimum ductility ratio, number of load cycles, sequence of application of load cycles and permissible reduction in strength at the end of loading. On the beam-column connection component level, the following performance are desirable: (i) ductile plastic hinge behavior under high shear stress, (ii) no congestion of transverse reinforcement for confinement and for shear, (iii) maintain concrete integrity under load reversals, and (iv) concrete damage contained within a relatively short hinging zone. These performance are

difficult to achieve with ordinary concrete, although some encouraging results have been obtained with fiber reinforced concrete. Desirable performance of the plastic hinge is not easy to translate directly into numerical quantities of materials property requirement. In general, however, it may be expected that the following properties of the concrete material in the plastic hinge should be advantageous:

- (i) high compression strain capacity to avoid loss of integrity by crushing,
- (ii) low tensile first cracking strength to initiate damage within the plastic hinge,
- (iii) high shear and spall resistance to avoid integrity loss by diagonal fractures, and
- (iv) enhanced mechanisms that increases inelastic energy dissipation.

In a recent study (50) the use of a strain-hardening ECC to achieve these objectives instead of increased shear steel reinforcement was investigated.

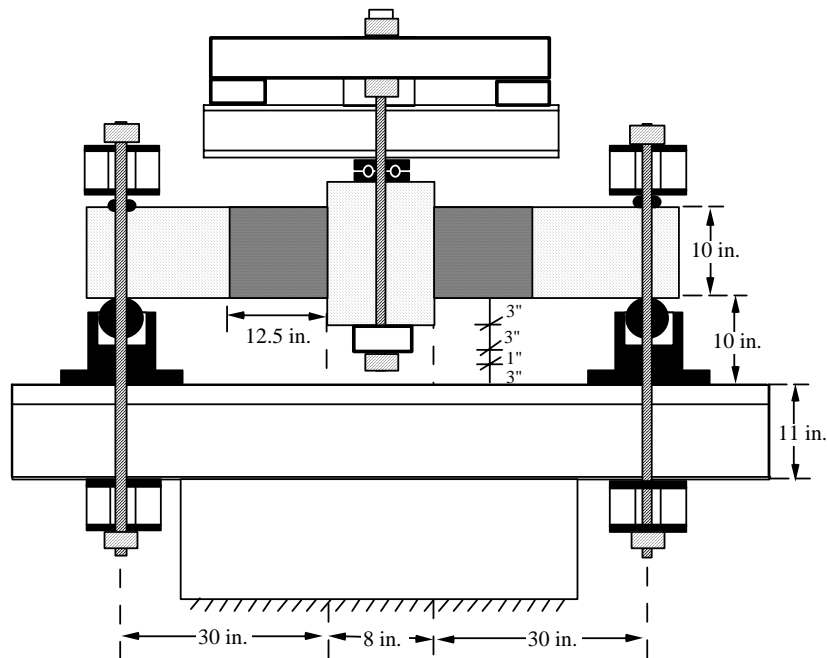


Fig. 21: Schematic of the experimental set-up

Experiment. The sub-assembly of R/C moment resisting frame selected for this testing program is shown schematically in Fig. 21. The test specimen represents two half beams connected to a stub column, in a strong column-weak beam configuration. The beams are simply supported at their ends to represent mid-span inflection points, under lateral loading of a framed structure.

Two specimens, one using plain concrete (PC) for the entire specimen and the other using ECC material in the plastic hinge zone and PC in the rest of the specimen, were tested. The so called non-ductile or ordinary detailing (Fig. 22) is used for both specimens to highlight the contribution of the ECC. For comparison, the seismic detailing is also shown in Fig. 22. Equal tension and compression steel ($\rho = 0.017$) is provided in form of two #6 bars each at the top and bottom of the

section. Closed shear stirrups (#2 bars) are provided at 4 in. spacing throughout the span. Shear span of the specimen is 30 in. and effective depth is 8.63 in. (Shear span to depth ratio = 3.5). The loading history used in this testing program consists of simple multiple steps of symmetric cycles of increasing displacement amplitude. The displacement controlled loading sequence used in this test is shown in Fig. 23.

Results and discussions. The load vs. deflection hysteretic behavior is shown in Fig. 24. For the PC hinge, the displacement ductility factor defined as the ratio of ultimate deflection (corresponding to a failure load that is about 20% lower than the maximum load carrying capacity) to yield deflection of about 4.8. For the ECC hinge, the displacement ductility factor increases to 6.4, with less amount of pinching and a much reduced rate of stiffness degradation (50). The cracking pattern (Fig. 25) was distinctly different with more cracking taking place in the plastic hinge zone with ECC rather than the zone outside as in the case of the PC control specimen. The damage is mostly in the form of diagonal multiple cracking in perpendicular direction. Unlike the control specimen which fail in a predominantly shear diagonal fracture, the ECC specimen fails by a vertical flexural crack at the interface between ECC plastic hinge zone and the plain concrete at the column face. No spalling was observed in the ECC hinge, whereas the concrete cover mostly disintegrated in the control. The cumulative energy over the load cycles for the two specimens are compared in Fig. 26 which shows that the ECC hinge absorbs about 2.8 times as much energy as the control. The control specimen does behave in a manner similar to the ECC hinge specimen in its range of deflection. However the ECC specimen far out-performs the control specimen in the deflection regime beyond 1.2".

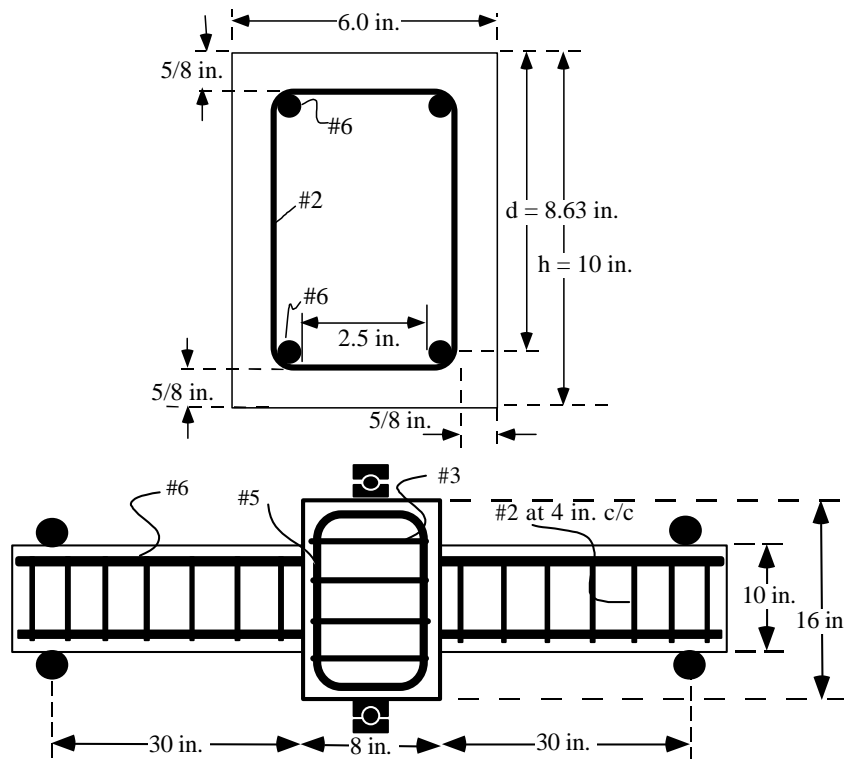


Fig. 22: Test configuration and reinforcement layout

RESEARCH NEEDS

Further research in ECCs are needed at both the material and structural levels. On the material level, additional property characterization and improvements are needed. These include, for example, the characterization of high and low cycle fatigue behavior, shrinkage behavior and freeze-thaw durability.

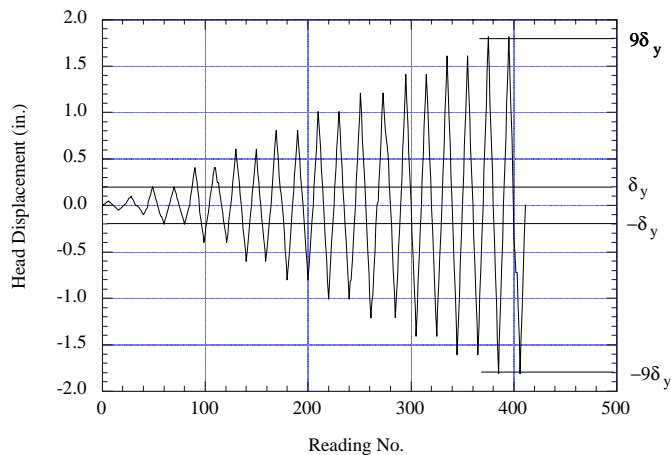


Fig. 23: Experimental data of loading sequence used in the test

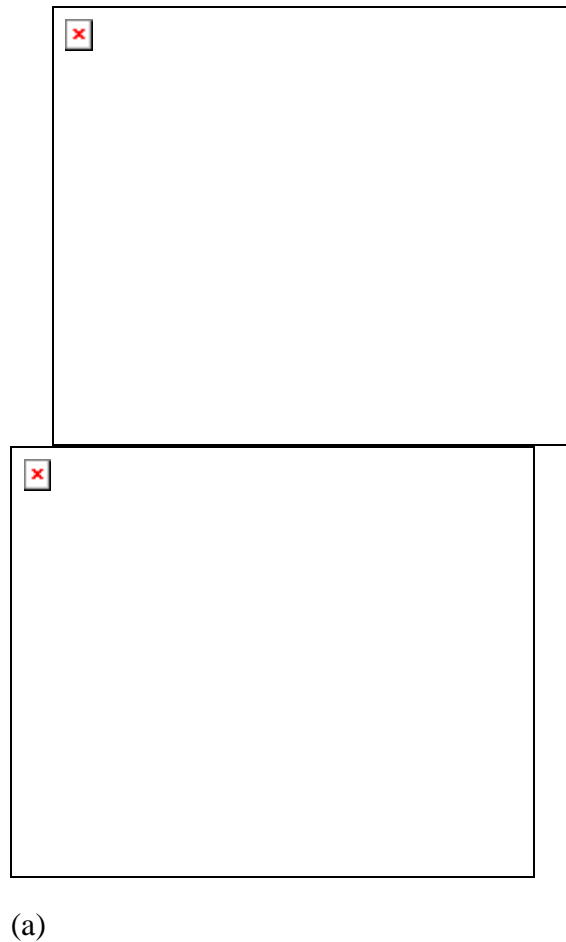


Fig. 24: Load vs. deflection response of (a) specimen with plain concrete plastic hinge, and (b) specimen with ECC plastic hinge

Research have been conducted in first crack stress and elastic modulus enhancement by addition of aggregates (30). This involves, however, careful design of matrix properties since the addition of aggregates leads to an increase in J_c which can rapidly increase the amount of fibers needed in satisfying the condition for pseudo strain hardening given in Eq. 6. Hence it is necessary to balance the various composite property needs by properly adjusting the material constituents. The delicate balance is greatly aided by the availability of the micromechanical models.

On a more micro-level, it is necessary to systematically investigate the tailoring of fiber, interface and matrix, guided by micromechanical principles. Fiber properties are continually improved, and new fiber types arise on an almost monthly basis. However, very few commercial fibers are especially geared towards applications in

cementitious composites. Manufacturers of advanced fibers tend to be more aware of the special needs in their fibers used in polymer matrix composites (FRP), ceramic matrix composites (CMC) and metal matrix composites (MMC). Unique requirements for reinforcement in cement based composites, apart from cost, needs to be researched and articulated. As an example, high fiber stiffness is much more important in FRP than in cement based composites. In contrast, high bending flexibility (translated into high tensile strain capacity) of the fiber is much more important in cement based composites, especially if the fibers are to be utilized in random orientations. Equally important are the fiber surface finish and treatment, both for fresh state processing purpose and for the hardened state mechanical properties. Fiber surface finish can affect the uniform dispersion of the fibers. Surface treatment, such as that by plasma, has been shown to effectively enhance interface bond property (30, 32).

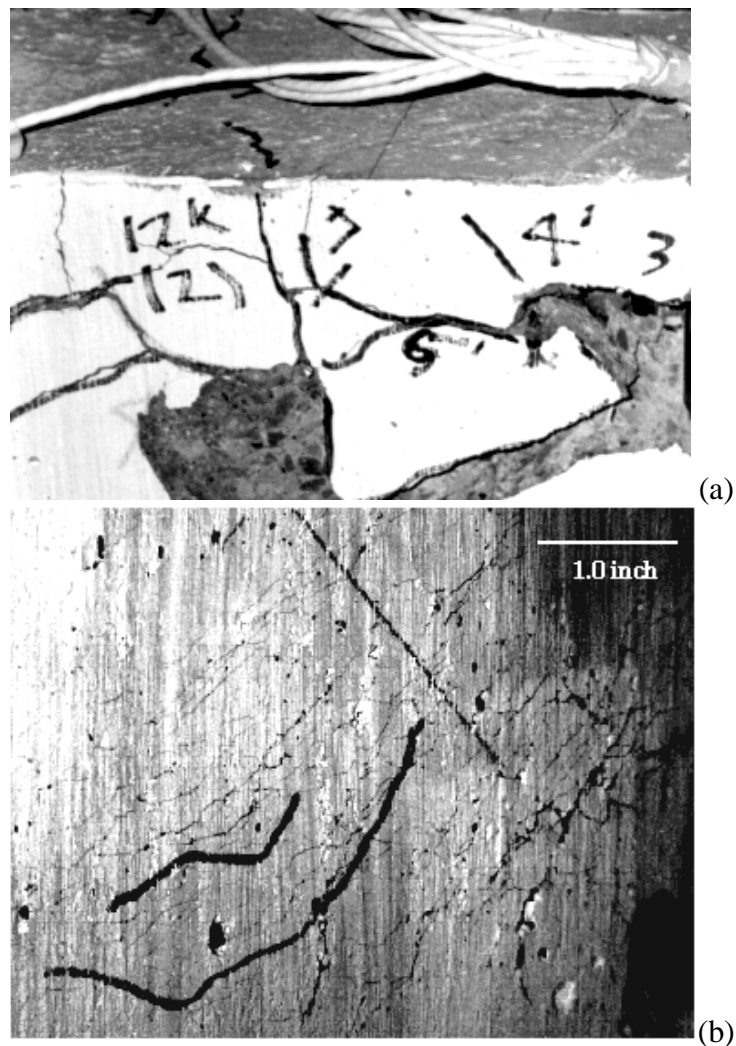


Fig. 25: Photograph of final failure, in the plastic hinge zone of

(a) control, and (b) ECC specimens

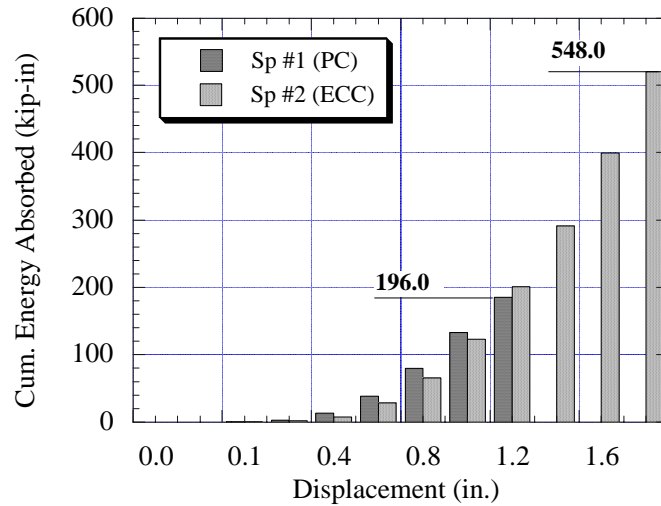


Fig. 26: Comparison of cumulative energy absorption vs. deflection of ECC hinge vs. the control

While micromechanical models are useful in guiding the detail manipulations of the fiber, matrix and interface properties, to achieve desirable composite properties, it is necessary to recognize the limitations of micromechanical models as well. For example, it is well known that the addition of second phase material in a composite can lead to changes in the microstructure and property of the matrix constituent (51) and these changes are sensitive to details of processing and the amount of the second phase additions. Cement based composites in general, and ECCs in particular, do not escape this phenomenon. Current micromechanical models typically do not recognize this fact, and straight forward use of these models can lead to erroneous results. Research into the quantification of the effects of fiber addition to cement matrix property changes is required.

Research in applications of ECCs are in an embryonic stage, and is badly needed. Field applications provide valuable feedback into the design of ECCs, both for fundamental mechanical and physical properties, as well as for properties needed for a particular application. Although the examples of applications of ECC in an element under intense shear loading, in a ECC layered R/C beam, and in a plastic-hinge zone of a beam-column connection described above demonstrate the value of ECC in structural performance enhancement, there is no question that both deeper studies of these applications, and broader studies of other ECC applications, are needed. As an example, the high strain capacity of ECC may suggest that the material may be very well suited for use as a patch material, wherein substrate constraint may create substantial imposed tensile strain due to drying shrinkage of repair material.

Continued research at the material level and structural level should be linked together, to provide feedback on each other so that progress on the material properties should be rapidly transferred to the structural performance level, and progress on structural behavior understanding should be quickly identified with specific material properties which can be affected by microstructure design. Fiber composites in general, and ECC in particular, provides ample opportunities to tailor material microstructure for structural performance in specific applications. Advances in such performance driven material design will no doubt require continued and sustained research, but the payoff can prove to be substantial also.

CONCLUDING REMARKS

This article reviews the various types of FRCs in use today, and suggest the need for developing a new class of FRCs which has the strain-hardening property but which can be processed with conventional equipment. It is demonstrated that such a material, termed engineered cementitious composites or ECCs, can be designed based on micromechanical principles. The result is a moderately low fiber volume fraction (<2%) composite which shows extensive strain-hardening, with strain capacity extending to several percent (up to 6% has been demonstrated), with compressive strength in the typical high strength concrete range (about 68.5 MPa), with fracture energy several times above typical FRCs (about 27 kJ/m²). Under bending and shear loads, the ECC beams show extensive ductile behavior both pre- and post-peak. In addition, the ECC material has indicated notch insensitivity in double edged uniaxial tensile specimens, suggesting that high reliability can be achieved in this type of composite. ECC has isotropic mechanical properties. Further improvement in ECCs, guided by micromechanical principles, are under investigations in the area of matrix modifications, interface tailoring, and fiber design. Because of the processing flexibility, the material can be used for pre-cast or cast-in-place structures, and broad classes of potential applications, such as those which require structural ductility, energy absorption, and crack width control under high strain imposition, are identified to be suitable to take advantage of the unique properties of ECCs. Some additional potential applications include

1. High energy absorption structures/devices:
 - EQ resistant structures – Columns, short span beam, beam-column connections
 - Seismic retrofits – shear walls, dampers
 - Steel structures – joints
 - Hybrid structures – steel/RC connections
2. Structures subject to impact loads:
 - Pavements – durability, reflective cracking
 - Building core element
 - Lightweight durable bridge decks
3. Large deformation structures:
 - Underground structures; conformability to soil deformation, leakage prevention
 - Concrete pipes
4. Others:

Permanent formwork; replacement of steel jacket of concrete columns.
Extruded products with structural capacity
Concrete cover for durability
Durable repair material
FRP reinforced concrete structure
Radio-active waste immobilization

ACKNOWLEDGMENTS

This article is partially based on an invited lecture given at the Engineering Foundation Conference on Advances in Cement and Concrete held in New Hampshire, June 1994. Additional material originally served as a contribution to the ACI/RILEM/ACBM 2nd International Workshop on High Performance Fiber Reinforced Cementitious Composites held in Michigan, June, 1995, has been included for completeness. Some materials presented here represent parts of doctoral theses research carried out by M. Maalej and D.K. Mishra, under the supervision of the author at the University of Michigan. Support of the Advanced Civil Engineering Materials Research Laboratory (ACE-MRL) by the Conoco Inc., Eternit Company, Kajima Corporation, NATO, Redco Company, Rocla Company, Shimizu Corporation, U.S. Gypsum Corporation, the U.S. National Science Foundation, and the U.S. National Research Council, are gratefully acknowledged.

REFERENCES

1. Balaguru, P.N. and Shah, S.P., Fiber Reinforced Cement Composites, McGraw Hill, 1992.
2. Krenchel, H., Synthetic Fibres for Tough and Durable concrete, in Developments in Fiber Reinforced Cement and Concrete, RILEM Symposium, R. N. Swamy, R. L. Wagstaffe and D.R. Oakley eds., 1986, pp. 333-338.
3. Krenchel, H. and Stang, H., Stable Microcracking in Cementitious Materials, in Proceedings of 2nd Int'l Symp. on Brittle Matrix Composites, Brandt, A.M., and I.H. Marshall, 1988, pp. 20-33.
4. Bentur, A. and Mindess, S., Fiber Reinforced Cementitious Composites, Elsevier Applied Science, 1990.
5. Batson, G., Jenkins, E. and Spatney, R., Steel Fibers As Shear Reinforcement In Beams, ACI Journal, 69(10) 1972, pp. 640-644.
6. Sharma, A. K., Shear Strength Of Steel Fiber Reinforced Concrete Beams, ACI Journal Proceedings, 83(4) 1986, pp. 624-628.
7. Swamy, R. N. and Bahia, H.M., The Effectiveness Of Steel Fibers As Shear Reinforcement, Concrete International, 1985 pp. 35-40.
8. Li, V.C., Ward, R. and Hamza, A.M., Steel And Synthetic Fibers As Shear Reinforcement, J. Materials, American Concrete Institute, 89(4) 1992, pp. 499-508.
9. Stang, H. and Aarre, T., Evaluation Of Crack Width In FRC With Conventional Reinforcement, Cement & Concrete Comp. 14(2) 1992, pp. 143-154.
10. Stang, H., Li, V.C. and Krenchel, H., Design And Structural Applications Of Stress-Crack Width Relations In Fiber Reinforced Concrete, RILEM J. of Materials and Structures, 28 1995, pp. 210-219.
11. Stang, H., Personal communication, 1994.
12. Horii, H. and Nanakorn, P., Fracture Mechanics Based Design Of SFRC Tunnel Lining, in Proceeding of JCI International Workshop on Size Effect in Concrete Structures, Oct. 31 - Nov. 2, 1993, Sendai, JAPAN, pp. 347-358.

13. Lankard, D.R. and Lease, D.H., Highly Reinforced Precast Monolithic Refractories, *Bulletin American Ceramic Society*, 61(7) 1982, pp. 728-732.
14. Schneider, B., Development Of SIFCON Through Applications, in "High Performance Fiber Reinforced Cement Composites", Reinhardt, H.W. and A.E. Naaman (Ed.), E&FN Spon, 1991, pp. 177-194.
15. Hackman, L.E., Farrell, M.B. and Dunham, O.O., Ultra High Performance Reinforced Concrete, in *Fiber Reinforced Concrete, Development and Innovations*, Eds. J.I. Daniel, and S.P. Shah, Published by ACI, SP-142, 1994, pp. 235-248.
16. Bentur, A. and Cree, R., Cement Reinforced With Steel Wool, *Int. J. Cem. Comp. & Ltwt. Concr.*, 9 1987, pp. 217-23.
17. Bache, H.H., Introduction To Compact Reinforced Composite, CBL Reprint No. 15, Aalborg Portland, 1987.
18. Naaman, A.E., Reinhardt, H.W. and Fritz, C., Reinforced Concrete Beams with a SIFCON Matrix, *ACI Structural J.*, 89 (1) 1992, pp. 79-88.
19. Jeong, S.M., Naaman, A.E. and Tan, K.H., Investigation Of Beams Partially Prestressed With Carbon Fiber Reinforced Composite Tendons, *Proceedings of the FIP XII Congress*, Washington, May 1994, pp. B56-B61.
20. Homrich, J. and Naaman, A.E., Stress-strain Properties of SIFCON in Compression, In "Fiber Reinforced Concrete, Properties and Applications", ed. S.P. Shah & G.B. Batson ACI SP-105, ACI, Detroit, 1987, pp. 283-304.
21. vanMier, J.G.M. and Timmers, G., Shear Fracture in SIFCON, in "High Performance Fiber Reinforced Cement Composites", Reinhardt, H.W. and A.E. Naaman (Ed.), E&FN Spon, 1991, pp. 518-528.
22. Li, V.C. and Leung, C.K.Y., Steady State And Multiple Cracking Of Short Random Fiber Composites, *ASCE J. of Engineering Mechanics*, 118(11) 1992, pp. 2246-2264.
23. Li, V.C. and Wu, H.C., Conditions For Pseudo Strain-Hardening In Fiber Reinforced Brittle Matrix Composites, *J. Applied Mechanics Review*, 45(8) 1992, pp. 390-398.
24. Li, V.C., From Micromechanics To Structural Engineering -- The Design Of Cementitious Composites For Civil Engineering Applications, *JSCE J. of Struc. Mechanics and Earthquake Engineering*, 10(2) 1993, pp. 37-48.
25. Marshall, B., Cox, B.N. and Evans, A.G., The Mechanics Of Matrix Cracking In Brittle Matrix Fiber Composites, *Acta Metall.*, 33(11) 1985, pp. 2013-2021.
26. Marshall, D. and Cox, B.N., A J-integral Method For Calculating Steady-State Matrix Cracking Stress In Composites, *Mechanics of Materials*, 7 1988, pp. 127-133.
27. Li, V.C., Post-Crack Scaling Relations For Fiber Reinforced Cementitious Composites, *ASCE J. of Materials in Civil Engineering*, 4(1) 1992, pp. 41-57.
28. Maalej, M., Li, V.C. and Hashida, T., Effect of Fiber Rupture On Tensile Properties Of Short Fiber Composites, *ASCE J. Engineering Mechanics*, 121(8) 1995, pp. 903-913.

29. Li, V.C. and Obla, K.H., Effect of Fiber Length Variation On Tensile Properties Of Carbon Fiber Cement Composites, *Int'l J. of Composites Engineering*, 4 (9) 1994, pp. 947 - 964.
30. Li, V.C., Mishra, D.K. and Wu, H.C., Matrix Design For Pseudo Strain-Hardening Fiber Reinforced Cementitious Composites, *RILEM J. Materials and Structures*, 28 (183) 1995, pp. 586-595.
31. Li, V.C., H.C. Wu, M. Maalej, D.K. Mishra and T. Hashida, Tensile Behavior of Cement Based Composites with Random Discontinuous Steel Fibers, *J. Amer. Ceramics Soc.*, 79 (1) 1996, pp. 74-78.
32. Li, V.C., Wu, H.C. and Chan, Y.W., Interfacial Property Tailoring For Pseudo Strain-Hardening Cementitious Composites, in *Advanced Technology on Design and Fabrication of Composite Materials and Structures*, Ed. Carpinteri and Sih, Kluwer Acad. Publ., Netherlands, 1995, pp. 261-268.
33. Li, V.C., Wang Y. and Backer, S., Effect of Inclining Angle, Bundling, And Surface Treatment On Synthetic Fiber Pull-Out From A Cement Matrix, *J. Composites*, 21(2) 1990, pp. 132-140.
34. Maalej, M., Hashida, T. and Li, V.C., Effect Of Fiber Volume Fraction On The Off-Crack-Plane Fracture Energy In Strain-Hardening Engineered Cementitious Composites", 78 (12) 1995, pp. 3369-3375.
35. Maalej, M. and Li, V.C., Flexural/tensile Strength Ratio In Engineered Cementitious Composites, *ASCE J. of Materials in Civil Engineering*, 6(4) 1994, pp. 513-528.
36. Li, V.C., Maalej, M. and Lim, Y.M., Fracture and Flexural Behavior In Strain-Hardening Cementitious Composites, in "Fracture of Brittle, Disorder Materials: Concrete, Rock and Ceramics", Eds. G. Baker and B.L. Karihaloo, 1995, pp. 101-114.
37. Li, V.C. and Hashida, T., Engineering Ductile Fracture In Brittle Matrix Composites, *J. of Materials Science Letters*, 12, 1993, pp. 898-901.
38. Li, V.C., Chan, C.M. and Leung, C.K.Y., Experimental Determination Of The Tension- Softening Curve In Cementitious Composites, *Cement and Concrete Research*, 17(3) 1987, pp. 441-452.
39. Csagoly, P.F., Design of Thin Concrete Deck Slabs By The Ontario Highway Bridge Design Code, Ontario Ministry of Transportation and Communications, 1979.
40. Fattuhi, N.I. and Huges, B.P., Ductility of Reinforced Concrete Corbels Containing Either Steel Fibers Or Stirrups, *ACI Materials J.*, 86(6) 1989, pp. 644-651.
41. Eligehausen, R. and Sawade, G., A Fracture Mechanics Based Description Of The Pull-Out Behavior Of Headed Studs Embedded In Concrete, in "Fracture Mechanics of Concrete Structures", 1989, pp. 281-299.
42. Lamberson, E.A. and Barker, J.M., Kishwaukee River Bridges, *Concrete International*, August, 1981, pp. 93-101.

43. Arakawa, T. and Ohno, K., Shear Tests Of Reinforced Concrete Beams By Special Type Of Loading, Transactions of the Architectural Institute of Japan, 57, pp. 581 - 584. (In Japanese)
44. Li, V.C., Mishra, D.K., Naaman, A.E., Wight, J.K., LaFave, J.M., Wu, H.C. and Inada, Y., On the Shear Behavior Of Engineered Cementitious Composites, J. of Advanced Cement Based Materials, 1(3) 1994, pp. 142-149.
45. Mufti, A. A., L.G. Jaeger, B. Bakht and L.D. Wegner, Experimental Investigation Of Fiber-Reinforced Concrete Deck Slabs Without Internal Steel Reinforcement, Can. J. Civ. Eng. 20 1993, pp. 398-406.
46. Maalej, M. and Li, V.C., Introduction Of Strain Hardening Engineered Cementitious Composites In The Design Of Reinforced Concrete Flexural Members For Improved Durability, J. Structures, American Concrete Institute, 92(2) 1995, pp. 167-176.
47. Tsukamoto, M., Tightness of Fiber Concrete, Darmstadt Concrete, Annual Journal on Concrete and Concrete Structures, 5, 1990, pp. 215-225.
48. Beeby, A.W., Cracking: What are Crack Width Limits For?, Concrete, 12(7) 1977-1978, pp. 31-33.
49. ACI Committee 224, Control of Cracking In Concrete Structures, ACI Manual of Concrete Practice Part 3-1991: Use of Concrete in Buildings-Design, Specifications, and Related Topics, American Concrete Institute, Detroit, 1991.
50. Mishra, D.K. and V.C. Li, Performance of a Ductile Plastic Hinge Designed With An Engineered Cementitious Composite, UMCEE Report No. 95-06, Feb., 1995.
51. Cohen, M.D., Goldman, A. and Chan, W.F., The Role Of Silica Fume In Mortar - Transition Zone Versus Bulk Paste Modification, Cement and Concrete Research, 24(1) 1994, pp. 95-98.